Photochemical & Photobiological Sciences

Optogenetic Rac1 engineered from membrane lipid-binding RGS-LOV for inducible lamellipodia formation

Journal:	*Photochemical & Photobiological Sciences*
Manuscript ID	PP-ART-11-2019-000434.R1
Article Type:	Paper
Date Submitted by the Author:	30-Jan-2020
Complete List of Authors:	Berlew, Erin; University of Pennsylvania, Bioengineering Kuznetsov, Ivan; University of Pennsylvania, Bioengineering Yamada, Keisuke; University of Pennsylvania, Bioengineering Bugaj, Lukasz; University of Pennsylvania, Bioengineering Chow, Brian; University of Pennsylvania, Bioengineering

Optogenetic Rac1 engineered from membrane lipid-binding RGS-LOV for inducible lamellipodia formation

Erin E. Berlew, Ivan A. Kuznetsov, Keisuke Yamada, Lukasz J. Bugaj, and Brian Y. Chow *

Department of Bioengineering, University of Pennsylvania, 210 South 33rd Street, Philadelphia, PA 19104, United States; (*) Correspondence: bchow@seas.upenn.edu

ABSTRACT:

We report the construction of a single-component optogenetic Rac1 (opto-Rac1) to control actin polymerization by dynamic membrane recruitment. Opto-Rac1 is a fusion of wildtype human Rac1 small GTPase to the C-terminal region of BcLOV4, a LOV (light-oxygen-voltage) photoreceptor that rapidly binds the plasma membrane upon blue-light activation via a direct electrostatic interaction with anionic membrane phospholipids. Translocation of the fused wildtype Rac1 effector permits its activation by GEFs (guanine nucleotide exchange factors) and consequent actin polymerization and lamellipodia formation, unlike in existing single-chain systems that operate by allosteric photo-switching of constitutively active Rac1 or the heterodimerization-based (i.e. two-component) membrane recruitment of a Rac1-activating GEF. Opto-Rac1 induction of lamellipodia formation was spatially restricted to the patterned illumination field and was efficient, requiring sparse stimulation duty ratios of ~1-2% (at the sensitivity threshold for flavin photocycling) to cause significant changes in cell morphology. This work exemplifies how the discovery of LOV proteins of distinct signal transmission modes can beget new classes of optogenetic tools for controlling cellular function.

INTRODUCTION:

Light-oxygen-voltage (LOV) flavoproteins [1-3] comprise the most ubiquitous class of photosensory proteins described to date [4, 5]. Their modularity in sensor-effector topology has given rise to great diversity in their photosensory signal transmission modes [5-12], and in turn, the discovery of LOV proteins with distinct signal transmission modes can beget new optogenetic modules for light-activated control over cell physiology [13, 14]. Recently, we reported one such novel class, the fungal (Regulator of G-protein Signaling) RGS-associated LOV proteins (RGS-LOV) [5], whose members possess a directly blue light-regulated and high-affinity interaction with anionic phospholipids and are reversibly recruited to the plasma membrane upon illumination in transducing cells as a result of this long-range electrostatic interaction [15].

Inducible translocation of a cytosol-sequestered protein to the plasma membrane is commonplace in optogenetics [16-20] to initiate signaling at the membrane by a fused effector (and likewise is commonplace with chemically induced dimerization (CID) [21, 22]. To the best of our knowledge, reported systems lack a direct interaction with the plasma membrane itself like RGS-LOV proteins, and instead rely on heterodimerization pairs that typically require multiple fluorescent protein tags and plasmids to titrate expression level for robust function [23-26]. Conversely, single-component membrane recruitment-based tools can be engineered with RGS-LOV, for example, as we recently demonstrated with opto-DHPH [27], which is a fusion of BcLOV4 from *Botrytis cinerea* [15] and the DHPH (Dbl-homology Pleckstrin-homology) domain of the Cdc-42 selective Intersectin GEF (guanine nucleotide exchange factor) to stimulate actin-mediated filopodial protrusions [28-31].

Here, we report the creation of opto-Rac1, a single-component tool for optogenetic induction of actin-mediated lamellipodial protrusions by membrane recruitment of human Rac1

small GTPase (**Figure 1**). Unlike existing optogenetic and chemogenetic tools that allosterically modulate constitutively active (CA) GTP-bound Rac1 [32, 33] or alter the subcellular localization of CA-Rac1 [34, 35] or Rac1-selective GEFs [36, 37] by heterodimerization-based membrane recruitment, opto-Rac1 modulates wildtype Rac1 by recruiting the inactive GDP-bound form to the membrane, where it is activated by GEFs [38] and initiates downstream actin polymerization through WAVE (WASP-family verprolin-homologous) protein-scaffolded interaction with Arp2/3 (actin-related proteins) regulatory complex [39-41]. The use of this wildtype or non-constitutively active effector minimized basal Rac1 activity in the dark, while still permitting effective photoinduction of lamellipodia formation that was spatially restricted to the illumination field and required relatively sparse epochs of illumination.

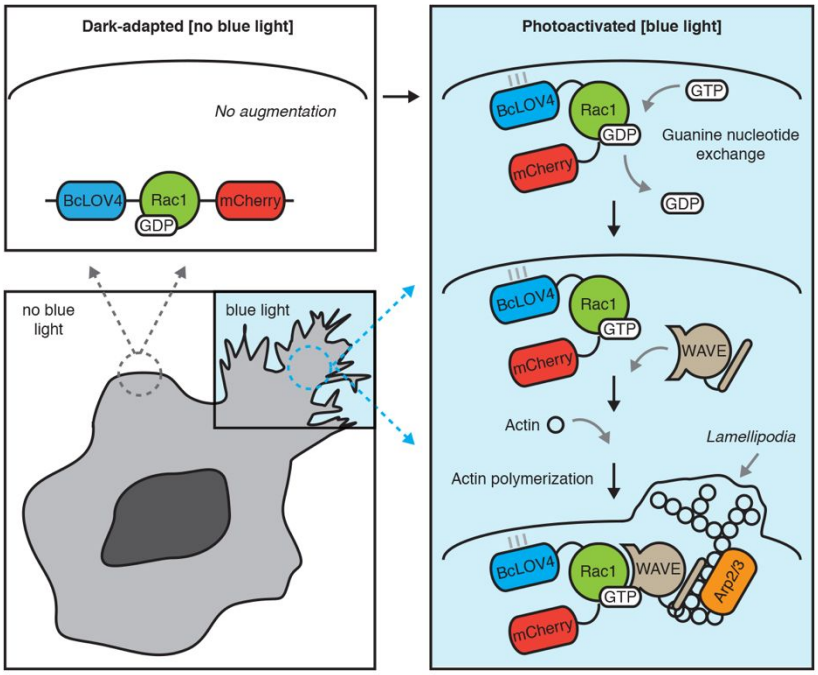

Figure 1: Optogenetic Rac1 (Opto-Rac1) photoinduction of lamellipodia formation by single-component dynamic membrane recruitment using BcLOV4. In the dark or absence of blue light, wildtype human Rac1 fused to BcLOV4 remains cytosolically sequestered and its GDP-bound inactive form. Upon illumination, BcLOV4 is directly recruited to the membrane through its light-regulated interaction with anionic membrane phospholipids. Rac1 is activated to its GTP-bound form by local GEF proteins, consequently initiating lamellipodia formation through interactions with the WAVE (scaffold) and Arp2/3 regulatory complex for actin polymerization.

MATERIALS AND METHODS:

[Genetic constructs]. Domain arrangement combinations of Rac1, BcLOV4, and mCherry (with a flexible $(GGGS)_2$ linker between each domain pair) were assembled by Gibson cloning using NEB HiFi DNA Assembly Master Mix (E2621) into the pcDNA3.1 mammalian expression vector under the CMV promoter. BcLOV4 and mCherry were amplified from their reported fusion (Addgene plasmid 114595) [15]. The DNA sequence of Rac1 (Genbank ID AAH04247.1) was human codon-optimized using the Integrated DNA Technologies (IDT) Codon Optimization Tool and ordered as a gBlock®, with a single C-terminal leucine residue (of the “CAAX”-motif) removed to prevent prenylation and membrane localization in dark-adapted fusions. The full

sequence is available in Supplementary Information (**Supplementary Figure 1**). The Rac1 constitutively active mutant was generated by QuikChange site-directed mutagenesis (Q665L, E695H, and N696H) based on previously reported mutations [33]. All genetic constructs were transformed into competent *E. coli* (New England Biolabs, C2984H). The DNA sequence of mKoKappa was human codon-optimized, ordered as a gBlock®, and assembled with BcLOV4 as described above. All sequences were verified by Sanger sequencing.

[Mammalian culture and transduction]. HEK293T (ATCC, CRL-3216) cells were cultured in D10 media composed of Dulbecco's Modified Eagle Medium with Glutamax (Invitrogen, 10566016), supplemented with 10% heat-inactivated fetal bovine serum (FBS) and Penicillin-Streptomycin at 100 U/mL. Cells were maintained in a 5% CO_2 water-jacketed incubator (Thermo/Forma 3110) at 37°C. Cells were seeded onto poly-D-lysine-treated glass bottom dishes (MatTek, P35GC-1.5-14-C) or into 24-well glass bottom plates (Cellvis, P24-1.5H-N) at 15-20% confluency. Cells were transfected at ~30-40% confluency 24 hours later using the TransIT-293 transfection reagent (Mirus Bio, MIR2700) according to manufacturer instructions. Cells were imaged 24–48 h post-transfection.

[Trypan blue staining]. 24 hours after transfection, cells were washed with PBS and incubated with 0.2% Trypan Blue solution (diluted 1:1 with PBS from 0.4% stock solution) for one minute. Trypan Blue solution was then aspirated, and cells were fixed with 4% paraformaldehyde for 10 minutes at room temperature. After fixation, plates were rinsed three times with PBS with agitation for five minutes per wash. Cells were then imaged at 20x magnification with brightfield illumination for three FOV per sample x 2 plates to count the number of stained vs. unstained cells for each construct.

[Optical hardware for cellular assays]. Fluorescence microscopy was performed on an automated Leica DMI6000B fluorescence microscope under Leica MetaMorph control, with a sCMOS camera (pco.edge), an LED illuminator (Lumencor Spectra-X), and a 63X oil immersion objective. Aligned excitation was filtered at the Lumencor for mCherry imaging (λ = 575/25 nm) and GFP imaging or for wide-field BcLOV4 stimulation (λ = 470/24 nm). mCherry-fused proteins were imaged with Chroma filters (T585lpxr dichroic and ET630/75nm emission filter). Camera exposure times ranged from 0.2-0.5 s. Cells were imaged in CO_2-independent media (phenol-free HBSS supplemented with 1% L-glutamine, 1% Penicillin-Streptomycin, 2% essential amino acids, 1% nonessential amino acids, 2.5% HEPES pH 7.0, and 10% serum).

The custom spatially patterned illuminator was (DMD) digital micromirror device-based and constructed from a digital light processor (DLP, Digital Light Innovations CEL5500), based on a design by others [42] (**Supplementary Figure 2**). All optics and optomechanics were from ThorLabs unless stated otherwise. A liquid light guide-coupled source (Mightex LCS-0455-3-22) was collimated into the DLP. The DLP output was infinity corrected with an additional lens, and the coupled through a side auxiliary port window of the microscope to gain direct access to the back of the objective, by using a custom K Type laser cube (Nuhsbaum, Inc.) with a shortpass dichroic mirror (λ < 900 nm). Digital masks were drawn in the DLP Light Commander software.

[Fluorescence imaging and optogenetic assays]. For dynamic membrane recruitment assessments, prenylated GFP was co-transfected as a membrane marker with Rac1::BcLOV4 fusions as previously described [15]. Following mCherry fluorescence imaging to assess the expression level and localization of the fusion proteins in the dark-adapted state, cells were illuminated with 5 s-long blue-light pulse whole-field to stimulate BcLOV4, and mCherry fluorescence images were captured every 200 ms to monitor membrane association of the protein during this stimulation epoch. GFP fluorescence was imaged immediately afterwards to visualize the marked membrane. mCherry fluorescence (500 ms excitation exposure) images

were then captured every 5 s in the absence of blue light to monitor protein dissociation from the membrane under thermal reversion. Membrane localization was measured by line section analysis and correlation with prenylated GFP in ImageJ and MATLAB as previously described [15].

For assays using spatially patterned illumination (see schematic protocol in **Supplementary Figure 3**), mCherry fluorescence was imaged every 15 s for up to 10 min. During this time, cells were periodically stimulated with DLP-patterned illumination (typically 25 μm-wide squares, ~25% cell area illuminated) with a 0.8 – 5% duty ratio range (or 0.25-1.5 s-long pulses once every 15-30 s). In the cases of mechanistic controls: for actin polymerization inhibition, cytochalasin D (5 mg/mL in DMSO, Millipore Sigma C2618) was added to cell media for a final concentration of 500 nM, 30 minutes prior to imaging; for Rac1-GEF inhibition, NSC23766 (Millipore Sigma SML0952) in phosphate-buffered saline (PBS) was added to cell media for a final concentration of 50 μM, one hour prior to imaging.

For normal handling, cells were passage, transfected, incubated and transported under standard laboratory lighting conditions, and then microscopy-based assays were conducted with room lights off after an initial 10-minute dark-adaptation period. All data reported were acquired under the normal handling conditions.

Under "stringent" conditions discussed in text, the cells were handled during all steps as prescribed by others for PA-Rac1 to reduce basal optogenetic activity [32]. Cell culture was performed under red safe-light conditions. Cells were transferred in completely opaque carriers. Assays were performed in dark rooms with all light-sources tuned off or baffled, including electronic displays and monitors [32].

[Data analysis]. Each data point was derived from an independent video, with N = 19-37 independent videos per condition. For each video, a cell within the illuminated region was selected and segmented (ImageJ) from the frame imaged at 0 seconds post-illumination and 120 seconds post-illumination. The researcher was blinded during segmentation to experimental condition to prevent bias. To compute the distance the cell had moved between the two timepoints, the average distance between segmented cell borders was calculated via a custom analysis Python script (schematized in **Supplementary Figure 3**). Statistical significance was assessed by the non-parametric Mann-Whitney U test, uncorrected for multiple comparisons.

RESULTS AND DISCUSSION:

In heterologous expression systems, BcLOV4 is dynamically recruited to the plasma membrane through a long-range electrostatic interaction between anionic membrane phospholipids and a polybasic amphipathic helix located between the LOV Jα-helical linker and its C-terminal domain of unidentified function (DUF) [15]. To engineer opto-Rac1, we screened domain arrangement orderings of mammalian codon-optimized BcLOV4, human Rac1, and a mCherry visualization tag, with a glycine/serine-rich flexible linker, $(GGGS)_2$, between the respective domain pairs (**Figure 2, Supplementary Figure 4**). To enable cytosolic sequestration of the Rac1 effector and limit membrane localization of BcLOV4-fusion proteins in the dark-adapted state, a single leucine residue was truncated from the Rac1 C-terminal prenylation site ("CLLL" or more generally "CAAX") [43]. These domain combinations were then screened in transfected HEK cells for protein expression uniformity, relative expression level, and light-activated translocation efficiency in response to whole-field illumination with blue light (**Figure 3**). In all experiments herein, cells were blue light-stimulated with a 15 mW/cm^2 irradiance, which is the half-saturation for flavin photocycling of BcLOV4-mCherry.

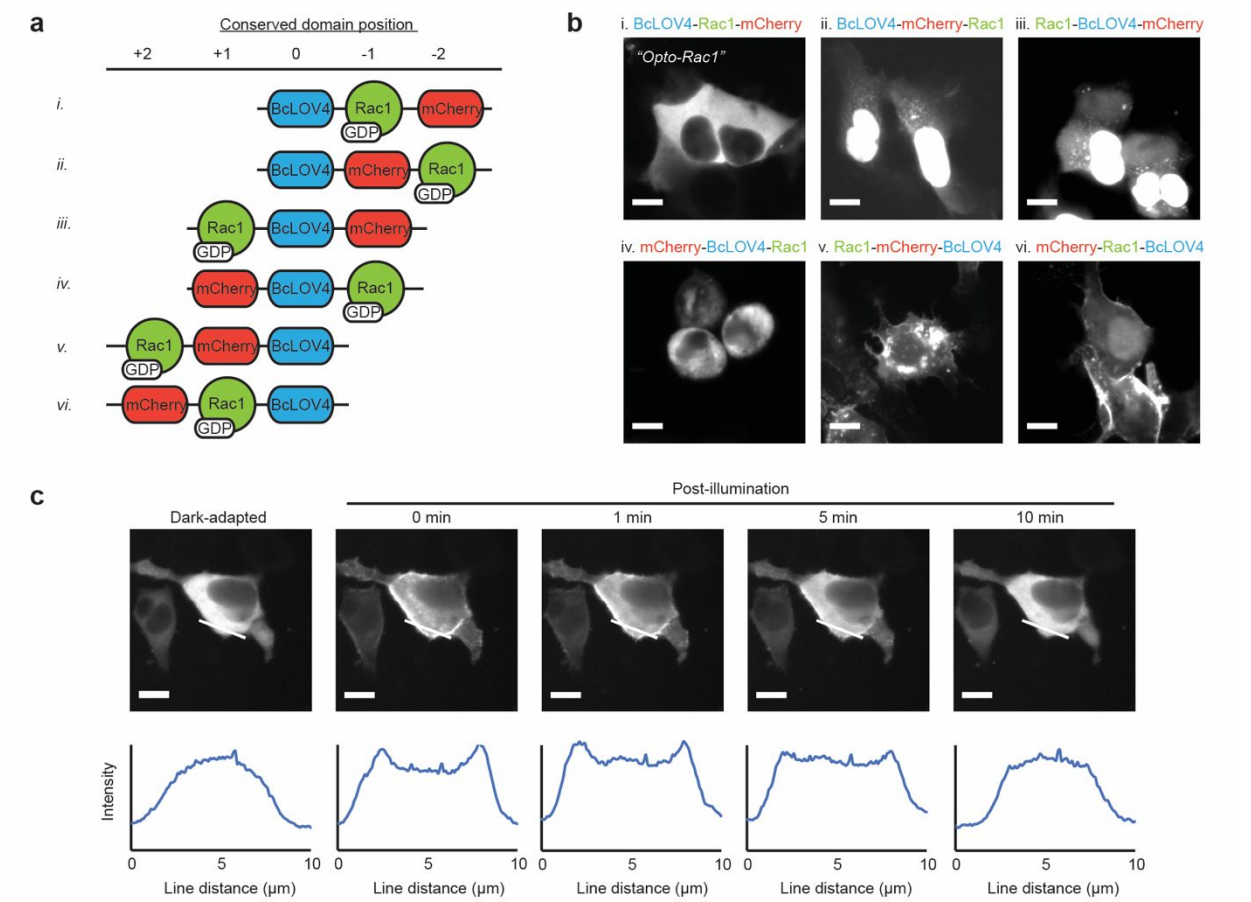

Figure 2: Molecular engineering of opto-Rac1. (a) Domain arrangement combinations of BcLOV4, wildtype human Rac1, and mCherry visualization tag that were tested. Domains were separated by flexible $(GGGS)_2$ linkers. Candidates were tested for relative expression level and translocation efficiency vs. BcLOV4-mCherry in transfected HEK cells. BcLOV4-Rac1-mCherry was ultimately selected as opto-Rac1 based on its uniform localization profile in the dark-adapted state and similar translocation efficiency to BcLOV4-mCherry. **(b)** Fluorescence micrographs showing representative expression patterns of the six arrangements in the dark-adapted state. **(c)** Dynamic membrane localization of opto-Rac1 is reversible under whole-field illumination. Top = Fluorescence micrograph, Scale = 10 μm. Bottom = Line section pixel intensity.

BcLOV4-Rac1-mCherry was chosen as opto-Rac1. This particular domain arrangement was uniformly distributed throughout the cytosol in the dark-adapted state (**Figure 2b, Supplementary Figure 4**), retained its ability to be reversibly recruited to the membrane upon illumination (**Figure 2c**) with similar efficiency to the BcLOV4-mCherry reference protein (**Figure 3b**). Other domain arrangements were not considered viable because their inducible membrane recruitment capabilities were reduced and they displayed undesirable expression profiles, evidenced by poor cell health (e.g. round morphology in domain arrangement iv), permanent localization to membrane or trans-Golgi network in the dark, or nuclear sequestration, the latter potentially from exposure of the Rac1 nuclear shuttling sequence [44] that is possible with disrupted prenylation [45]. The observed nuclear sequestration was unlikely to depend on cell cycle phase [46], since it is the dominant phenotype observed in an unsynchronized population for domain arrangements ii and iii (**Supplementary Figure 4**).

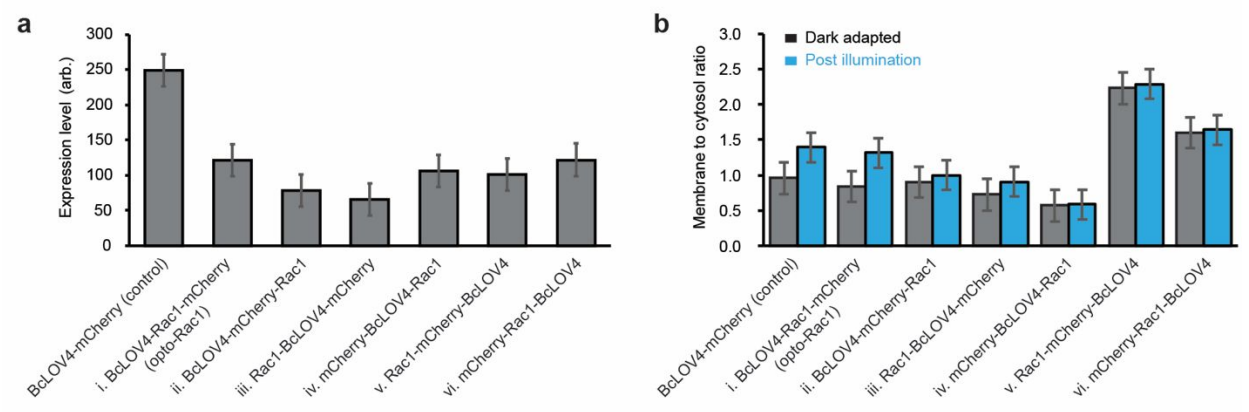

Figure 3: Population analysis of domain arrangement combinations. **(a)** Relative expression level vs. BcLOV4-mCherry control with no effector. **(b)** Ratio of membrane-localized vs. cytosolic protein for the engineered arrangements (normalized vs. BcLOV4-mCherry control) in the dark-adapted and blue light-illuminated state. N = 25 – 35 each. Mean ± standard error.

The membrane localization in the dark-adapted state observed when BcLOV4 is at the C-terminus of the chimera (domain arrangements v. and vi.) suggests that such configurations are disfavored when engineering fusion proteins. A similar "permanently lit"-like phenotype was seen when only a fluorescent protein was placed at the N-terminus as a membrane signaling-inert fusion partner (mKoκ-BcLOV4, **Supplementary Figure 5**). It is possible that fused N-terminal effectors may disrupt the known dark-state inhibition of lipid-binding by the N-terminal region of BcLOV4 [15]. Future work in high-resolution structures of BcLOV4 may reveal how certain configurations differ in their exposure of motifs (nuclear localization, lipid binding, etc.) that impact their respective distribution patterns. It should be noted that opto-Rac1 could not be solubly produced by bacterial overexpression.

Next, to test optogenetic function for spatially precise induction of lamellipodia formation, cells expressing opto-Rac1 were stimulated with spatially patterned blue light using a digital micromirror device (**Figures 4 and 5**) to emulate a sensory activation gradient. Because BcLOV4 undocks from the membrane within approximately one minute in the dark [15, 47], cells were provided a brief stimulation pulse every 30-60 seconds. Sprawling sheet-like lamellipodial protrusions were rapidly and selectively initiated in the blue light-illuminated field and remained largely confined to the spatial field upon reaching the boundary (**Figure 4** and **Supplementary Video 1**). Thus, opto-Rac1 induction of lamellipodia formation is spatially restricted.

We assessed the phenotypic response to different stimulation duty ratios to gauge the functional efficiency of opto-Rac1 and guide experimental parameters for future use. Duty ratio (ϕ) was chosen as the "sensitivity" parameter because it is easier to precisely control optical stimulation timing than intensity over time. The 15 mW/cm^2 irradiance was chosen as it is sufficient to saturate flavin photocycling, but this photochemical threshold at the protein-level was not exceeded to avoid photobleaching or compensating for inefficient optogenetic function at the cell signaling level. We quantified the extent of induced lamellipodia formation (**Figure 5**) as the average movement of the stimulated cell boundary over the first two minutes, since protrusions were clearly observable during this initial post-induction period and the spatial confinement of lamellipodia induction to the illumination field decreases the average movement over longer periods. Opto-Rac1 performed consistently at $\phi =$ 1.6% duty ratio, which for context is in the low end of the duty ratio range of $\phi \sim$ 2.5 – 20% that has been reported for related tools for small GTPase signaling with blue light photoreceptors [29-31, 37, 48]. Thus, the optogenetic

215 efficiency of opto-Rac1 is sufficient to perform reliably on commonplace microscopy setups
216 without major photobleaching risks.

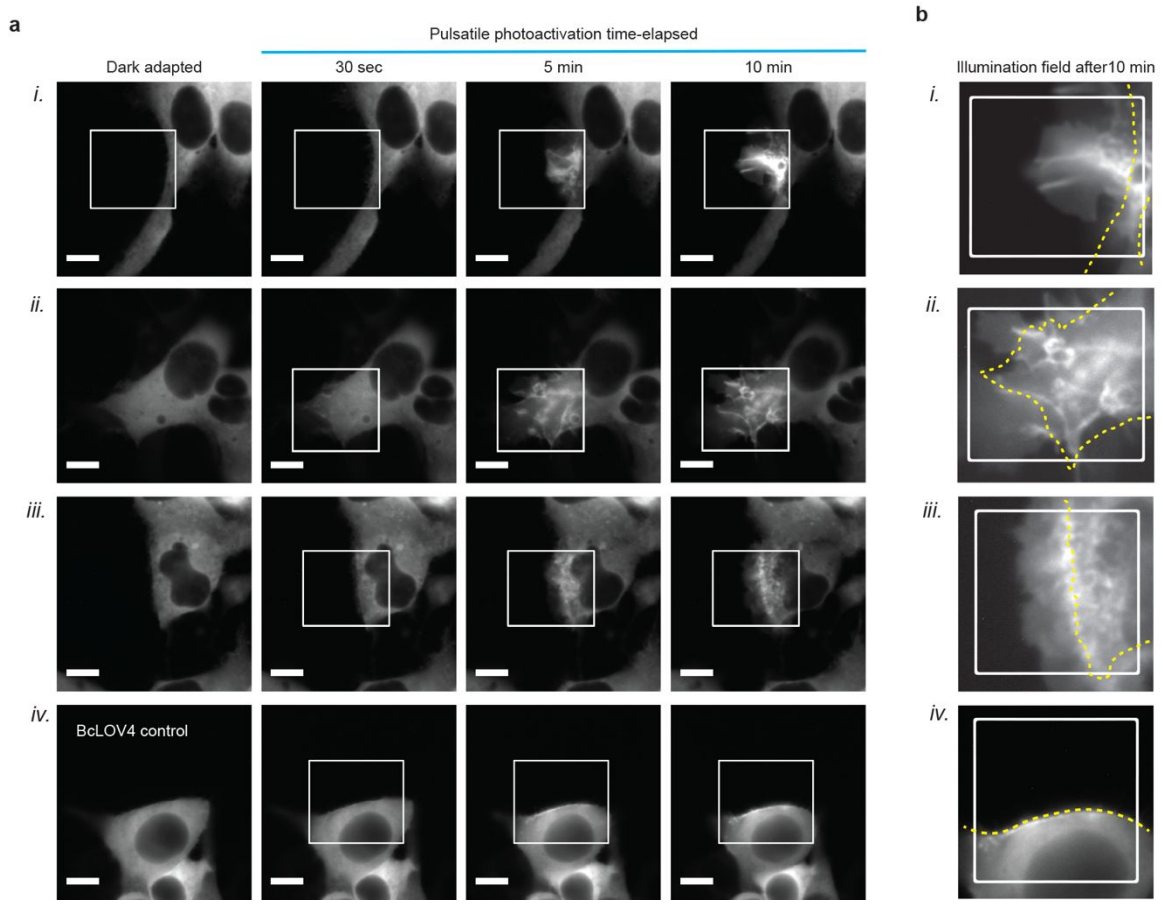

Figure 4. Spatially precise induction of lamellipodia formation by opto-Rac1 (a) Fluorescence micrographs of three different transfected HEK cells and a BcLOV4 control. Protrusions are rapidly formed in the patterned illumination field for opto-Rac1, and remain largely restricted to the field even many minutes after reaching the edge. Opto-Rac1 also accumulates selectively within the field in an actin network-dependent manner (refer also to Figure 6). No protrusions are observed for the effector-less control. Scale = 10 µm. **(b)** Region of interest (ROI) selection around the illumination field of view after 10 minutes of pulsatile stimulation show sheet-like protrusions. Indices i-iv correspond to those in panel a, with auto-adjusted levels for the ROI. White box = illumination field. Dotted yellow line = mask of original cell boundary. (a-b) λ = 455 nm @ 15 mW/cm^2, 1.6 – 5.0% duty ratio.

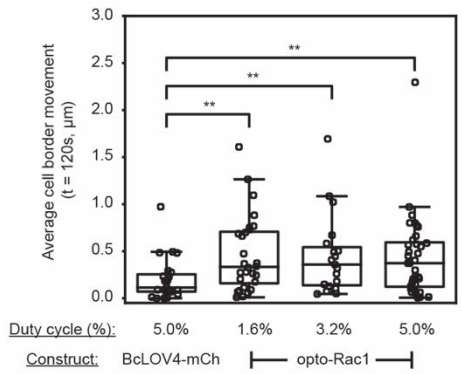

Figure 5. Efficient opto-Rac1 induction of lamellipodia formation. Lamellipodia formation in response to stimulation duty cycles, with irradiance fixed at the saturation threshold for flavin photocycling. Phenotypic response was quantified by average distance of cell border movement in the illumination field after two minutes. N = 19 – 37 independent videos each. Mann-Whitney U test: (*) $p < 0.05$, (**) $p < 0.01$ vs. BcLOV4-mCherry control (no Rac1 effector). λ = 455 nm @ 15 mW/cm^2.

To confirm that the wildtype Rac1 domain can be recruited to the membrane in its inactive GDP-bound form as proposed, we performed the spatially patterned induction experiments in the presence of a Rac1-GEF inhibitor NSC 23766 [49, 50], with a high $\phi =$ 5% to ensure robust photochemical activation. Opto-Rac1 still selectively bound the membrane in illumination field, but lamellipodia formation was suppressed by this pharmacological inhibition (**Figure 6**). This finding confirms that its membrane recruitment is GEF-independent and indicates that the wildtype effector domain is in its inactive or GDP-bound when opto-Rac1 is initially recruited to the membrane. This signaling mode is consistent with single-molecule tracking studies showing that membrane localization of Rac-GDP precedes GEF-activation in natural Rac1 signaling, and is sufficient for actin polymerization [38].

Lamellipodia formation was also inhibited in the presence of the actin polymerization inhibitor cytochalasin D [51], confirming that the cytoskeletal rearrangements were actin-mediated and not a spurious byproduct of other Rac1 signaling pathways or protein accumulation at the inner leaflet (**Figure 6**). Opto-Rac1 did not accumulate strongly in the illumination field in the presence of either inhibitor, unlike when actin polymerization is possible (**Figure 4**), and thus the latter observed accumulation stems from opto-Rac1 binding to a polymerized actin network.

The opto-Rac1 signaling mechanism is distinct from previously reported genetically encoded approaches for inducible Rac1 activity, which have used Rac1-activating GEFs or constitutively active (CA) proteins mutated to eliminate inhibitory interactions with GDI (guanosine nucleotide dissociation inhibitor) and GAPs (GTPase-activating protein) [32-37]. While membrane recruitment systems have not yet been reported using wildtype Rac1 effector (vs. CA-Rac1 or indirect Rac1-GEFs), its use clearly permits effective opto-Rac1 signaling and suggests that basal GEF levels are sufficient to support signaling in response to rapid increases in membrane concentration of GDP-bound Rac1. It should be noted that mutation of the Rac1 domain in opto-Rac1 to CA-Rac1 [33] (corresponding to the GDI-interaction site, Q61L, and the GAP-interaction sites, E91H and N92H) was toxic with evidence of basal activity (**Supplementary Figure 6**). Thus, the use of wildtype Rac1 effector contributes to the optogenetic efficacy, possibly by reducing basal activity of opto-Rac1, which was negligible under normal laboratory condition (without precautions for blue light-exposure other than brief assay dark-adaptation period) that were less stringent than reported precautions needed to limit basal activity of PA-Rac1, where all cell handling and assays are conducted in darkness (including baffling electronic displays) [32].

Opto-Rac1 contributes to the overall optogenetic toolbox for controlling Rac1 signaling, whose members differ in their respective GEF-input signal integration and their consequent downstream effects [36, 52, 53]. For example, optogenetic GEF-induced signaling is biased by the native preferences of the effector, whereas the wildtype Rac1 effector integrates multiple GEF inputs and conversely, a chimeric CA-Rac1 effector drives downstream processes in a direct GEF-independent manner. Further, the gain-of-function by an engineered GEF saturates at the endogenous GTPase concentration, whereas the maximum for an engineered GTPase itself corresponds to the enhanced GTPase concentration net of overexpression [54]. Thus, expanding the toolbox offers tailored approaches to probe Rac1 signaling. Opto-Rac1 here perhaps recapitulates increases in concentration (e.g. by transcriptional up-regulation, nuclear export, etc.) on very rapid timescales while still integrating natural GEF inputs that influence its output.

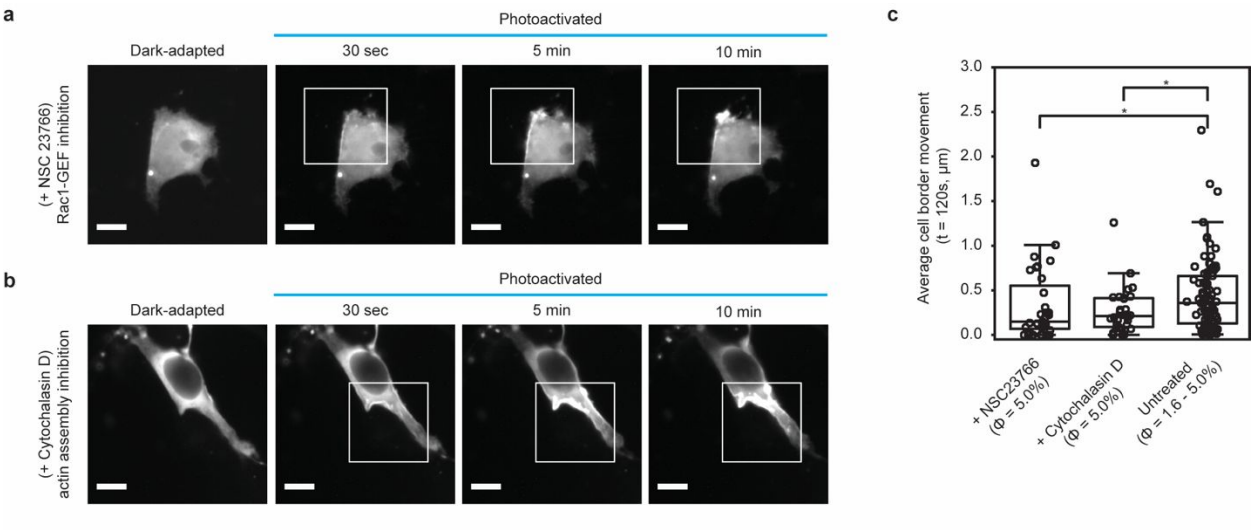

Figure 6. Pharmacological inhibition of opto-Rac1 activity to confirm mechanism of optogenetic control. Optogenetic signaling proceeds by GEF-activation of GDP-bound wildtype Rac1 upon membrane localization, followed by downstream actin polymerization. **(a-b)** Fluorescence micrographs of transfected HEK cells expressing opto-Rac1, treated with the (a) Rac1- GEF inhibitor NSC23766 and (b) the actin polymerization inhibitor cytochalasin D. Opto-Rac1 accumulates at the membrane within the patterned illumination field (box) but does not induce lamellipodia formation. λ = 455 nm @ 15 mW/cm^2, 5% duty ratio. Scale = 10 µm. **(c)** Population level data to quantify pharmacological suppression of opto-Rac1 activity. Mann Whitney U test (*) $p < 0.05$. N = 31 (+NSC23766), N = 30 (+cytochalasin D) independent videos each. Untreated samples represent the same data as in Figure 5.

CONCLUSION:

In summary, we have created a single-component optogenetic Rac1 that potently initiates actin polymerization and highly focal lamellipodia formation by blue light-activated membrane recruitment of wildtype Rac1 GTPase itself. This work demonstrates how BcLOV4 as a protein technology is a versatile and powerful module for engineering chimeric optogenetic tools to control signaling of membrane-associated proteins, and highlights the importance of establishing the structure-function of novel signal transmission modes, such as the foundational light-regulated protein-lipid interaction described here, that are employed by the ubiquitous and inherently modular LOV domain photoreceptors.

AUTHOR CONTRIBUTIONS:

EEB designed genetic constructs, designed experiments, and conducted all experiments. IAK designed experiments, contributed to all experiments, constructed the patterned illumination system, and performed the blinded data analysis. KY assisted with molecular cloning and cellular assays. LJB and BYC coordinated all research. All authors contributed to data analysis and manuscript preparation.

ACKNOWLEDGEMENTS:

We dedicate this manuscript in memory of Winslow R. Briggs, a true luminary in photosensory biology. We thank the Chris Fang-Yen Laboratory for assistance with constructing the spatially patterned illuminator. BYC acknowledges the support of National Science Foundation (NSF) Systems and Synthetic Biology (MCB 1652003), NIH/National Institute on Drug Abuse (R21 DA040434), and NIH/National Institute of Neurological Disorders and Stroke (NINDS) (R01 NS101106). LJB acknowledges the support of the W.W. Smith Charitable Trust, ACS-SEAS Discovery Grant, and NIH/National Institute of General Medical Sciences (R21 GM132831-01). IAK acknowledges the fellowship support of the Paul and Daisy Soros Fellowship for New Americans and the NIH/National Institutes of Mental Health (NIMH) Ruth L. Kirchstein NRSA (F30 MH122076-01).

REFERENCES:

1. E. Huala, P. W. Oeller, E. Liscum, I.-S. Han, E. Larsen and W. R. Briggs, Arabidopsis NPH1: A Protein Kinase with a Putative Redox-Sensing Domain, *Science*, 1997, **278**, 2120.
2. W. R. Briggs, Phototropism: Some History, Some Puzzles, and a Look Ahead, *Plant physiology*, 2014, **164**, 13.
3. S. Crosson, S. Rajagopal and K. Moffat, The LOV domain family: photoresponsive signaling modules coupled to diverse output domains, *Biochemistry*, 2003, **42**, 2-10.
4. A. Losi and W. Gärtner, Solving Blue Light Riddles: New Lessons from Flavin-binding LOV Photoreceptors, *Photochemistry and photobiology*, 2016, **93**, 141-158.
5. S. T. Glantz, E. J. Carpenter, M. Melkonian, K. H. Gardner, E. S. Boyden, G. K. Wong and B. Y. Chow, Functional and topological diversity of LOV domain photoreceptors, *Proceedings of the National Academy of Sciences of the United States of America*, 2016, **113**, E1442-1451.
6. J. Herrou and S. Crosson, Function, structure and mechanism of bacterial photosensory LOV proteins, *Nature reviews. Microbiology*, 2011, **9**, 713-723.
7. S. M. Harper, L. C. Neil and K. H. Gardner, Structural basis of a phototropin light switch, *Science*, 2003, **301**, 1541-1544.
8. A. I. Nash, R. McNulty, M. E. Shillito, T. E. Swartz, R. a. Bogomolni, H. Luecke and K. H. Gardner, Structural basis of photosensitivity in a bacterial light-oxygen-voltage/helix-turn-helix (LOV-HTH) DNA-binding protein, *Proceedings of the National Academy of Sciences of the United States of America*, 2011, **108**, 9449-9454.
9. R. P. Diensthuber, M. Bommer, T. Gleichmann and A. Möglich, Full-length structure of a sensor histidine kinase pinpoints coaxial coiled coils as signal transducers and modulators, *Structure*, 2013, **21**, 1127-1136.
10. A. M. Weber, J. Kaiser, T. Ziegler, S. Pilsl, C. Renzl, L. Sixt, G. Pietruschka, S. Moniot, A. Kakoti, M. Juraschitz, S. Schrottke, L. Lledo Bryant, C. Steegborn, R. Bittl, G. Mayer and A. Möglich, A blue light receptor that mediates RNA binding and translational regulation, *Nature Chemical Biology*, 2019, **15**, 1085-1092.
11. K. S. Conrad, A. M. Bilwes and B. R. Crane, Light-Induced Subunit Dissociation by a LOV domain Photoreceptor from Rhodobacter sphaeroides, *Biochemistry*, 2013, **52**, 378-391.
12. C. H. Chen, B. S. DeMay, A. S. Gladfelter, J. C. Dunlap and J. J. Loros, Physical interaction between VIVID and white collar complex regulates photoadaptation in Neurospora, *Proc Natl Acad Sci USA*, 2010, **107**, 16715-16720.
13. A. Losi, K. H. Gardner and A. Möglich, Blue-Light Receptors for Optogenetics, *Chemical Reviews*, 2018, **118**, 10659-10709.
14. J. M. Christie, J. Gawthorne, G. Young, N. J. Fraser and A. J. Roe, LOV to BLUF: flavoprotein contributions to the optogenetic toolkit, *Mol Plant*, 2012, **5**, 533-544.
15. S. T. Glantz, E. E. Berlew, Z. Jaber, B. S. Schuster, K. H. Gardner and B. Y. Chow, Directly light-regulated binding of RGS-LOV photoreceptors to anionic membrane phospholipids, *Proceedings of the National Academy of Sciences*, 2018, **115**, E7720-E7727.
16. M. J. Kennedy, R. M. Hughes, L. A. Peteya, J. W. Schwartz, M. D. Ehlers and C. L. Tucker, Rapid blue-light-mediated induction of protein interactions in living cells, *Nat Meth*, 2010, **7**, 973-975.
17. G. Guntas, R. A. Hallett, S. P. Zimmerman, T. Williams, H. Yumerefendi, J. E. Bear and B. Kuhlman, Engineering an improved light-induced dimer (iLID) for controlling the localization and activity of signaling proteins, *Proceedings of the National Academy of Sciences*, 2015, **112**, 112.

18. D. Strickland, Y. Lin, E. Wagner, C. M. Hope, J. Zayner, C. Antoniou, T. R. Sosnick, E. L. Weiss and M. Glotzer, TULIPs: tunable, light-controlled interacting protein tags for cell biology, *Nat. Methods*, 2012, **9**, 379-384.
19. A. A. Kaberniuk, A. A. Shemetov and V. V. Verkhusha, A bacterial phytochrome-based optogenetic system controllable with near-infrared light, *Nature methods*, 2016, **13**, 591-597.
20. A. Levskaya, O. D. Weiner, W. A. Lim and C. A. Voigt, Spatiotemporal control of cell signalling using a light-switchable protein interaction, *Nature*, 2009, **461**, 997-1001.
21. R. DeRose, T. Miyamoto and T. Inoue, Manipulating signaling at will: chemically-inducible dimerization (CID) techniques resolve problems in cell biology, *Pflugers Arch*, 2013, **465**, 409-417.
22. S. Voß, L. Klewer and Y.-W. Wu, Chemically induced dimerization: reversible and spatiotemporal control of protein function in cells, *Current Opinion in Chemical Biology*, 2015, **28**, 194-201.
23. L. Duan, J. Hope, Q. Ong, H.-Y. Lou, N. Kim, C. McCarthy, V. Acero, M. Z. Lin and B. Cui, Understanding CRY2 interactions for optical control of intracellular signaling, *Nature communications*, 2017, **8**, 547.
24. R. A. Hallett, S. P. Zimmerman, H. Yumerefendi, J. E. Bear and B. Kuhlman, Correlating in Vitro and in Vivo Activities of Light-Inducible Dimers: A Cellular Optogenetics Guide, *ACS synthetic biology*, 2016, **5**, 53-64.
25. S. P. Zimmerman, R. A. Hallett, A. M. Bourke, J. E. Bear, M. J. Kennedy and B. Kuhlman, Tuning the Binding Affinities and Reversion Kinetics of a Light Inducible Dimer Allows Control of Transmembrane Protein Localization, *Biochemistry*, 2016, **55**, 5264-5271.
26. P. Hannanta-Anan and B. Y. Chow, Optogenetic Inhibition of Gαq Protein Signaling Reduces Calcium Oscillation Stochasticity, *ACS synthetic biology*, 2018, **7**, 1488-1495.
27. P. Hannanta-Anan, S. T. Glantz and B. Y. Chow, Optically inducible membrane recruitment and signaling systems, *Current Opinion in Structural Biology*, 2019, **57**, 84-92.
28. L. Valon, F. Etoc, A. Remorino, F. di Pietro, X. Morin, M. Dahan and M. Coppey, Predictive Spatiotemporal Manipulation of Signaling Perturbations Using Optogenetics, *Biophysical Journal*, 2015, **109**, 1785-1797.
29. S. de Beco, K. Vaidžiulytė, J. Manzi, F. Dalier, F. di Federico, G. Cornilleau, M. Dahan and M. Coppey, Optogenetic dissection of Rac1 and Cdc42 gradient shaping, *Nature communications*, 2018, **9**, 4816-4816.
30. P. R. O'Neill, V. Kalyanaraman and N. Gautam, Subcellular optogenetic activation of Cdc42 controls local and distal signaling to drive immune cell migration, *Mol Biol Cell*, 2016, **27**, 1442-1450.
31. O. Van Geel, R. Hartsuiker and T. W. J. Gadella, Increasing spatial resolution of photoregulated GTPases through immobilized peripheral membrane proteins, *Small GTPases*, 2018, DOI: 10.1080/21541248.2018.1507411, 1-10.
32. Y. I. Wu, X. Wang, L. He, D. Montell and K. M. Hahn, Spatiotemporal control of small GTPases with light using the LOV domain, *Methods in enzymology*, 2011, **497**, 393-407.
33. Y. I. Wu, D. Frey, O. I. Lungu, A. Jaehrig, I. Schlichting and B. H. Kuhlman, K.M., A genetically encoded photoactivatable Rac controls the motility of living cells, *Nature*, 2009, **461**, 104-108.
34. T. Inoue, W. D. Heo, J. S. Grimley, T. J. Wandless and T. Meyer, An inducible translocation strategy to rapidly activate and inhibit small GTPase signaling pathways, *Nature methods*, 2005, **2**, 415-418.
35. F. Castellano, P. Montcourrier and P. Chavrier, Membrane recruitment of Rac1 triggers phagocytosis, *Journal of Cell Science*, 2000, **113**, 2955.

36. B. R. Graziano, D. Gong, K. E. Anderson, A. Pipathsouk, A. R. Goldberg and O. D. Weiner, A module for Rac temporal signal integration revealed with optogenetics, *The Journal of Cell Biology*, 2017, **216**, 2515.
37. A. Remorino, S. De Beco, F. Cayrac, F. Di Federico, G. Cornilleau, A. Gautreau, M. C. Parrini, J. B. Masson, M. Dahan and M. Coppey, Gradients of Rac1 Nanoclusters Support Spatial Patterns of Rac1 Signaling, *Cell reports*, 2017, **21**, 1922-1935.
38. S. Das, T. Yin, Q. Yang, J. Zhang, Y. I. Wu and J. Yu, Single-molecule tracking of small GTPase Rac1 uncovers spatial regulation of membrane translocation and mechanism for polarized signaling, *Proceedings of the National Academy of Sciences*, 2015, **112**, E267.
39. S.-T. Sit and E. Manser, Rho GTPases and their role in organizing the actin cytoskeleton, *Journal of Cell Science*, 2011, **124**, 679.
40. A. Y. Pollitt and R. H. Insall, WASP and SCAR/WAVE proteins: the drivers of actin assembly, *Journal of cell science*, 2009, **122**, 2575-2578.
41. T. D. Pollard, Regulation of Actin Filament Assembly by Arp2/3 Complex and Formins, *Annual review of biophysics and biomolecular structure*, 2007, **36**, 451-477.
42. N. F. Trojanowski and C. Fang-Yen, in *C. elegans: Methods and Applications*, eds. D. Biron and G. Haspel, Humana Press, Totowa, NJ, 2015, DOI: 10.1007/978-1-4939-2842-2_9, pp. 105-119.
43. P. J. Roberts, N. Mitin, P. J. Keller, E. J. Chenette, J. P. Madigan, R. O. Currin, A. D. Cox, O. Wilson, P. Kirschmeier and C. J. Der, Rho Family GTPase modification and dependence on CAAX motif-signaled posttranslational modification, *The Journal of biological chemistry*, 2008, **283**, 25150-25163.
44. C. C. Lanning, J. L. Daddona, R. Ruiz-Velasco, S. H. Shafer and C. L. Williams, The Rac1 C-terminal Polybasic Region Regulates the Nuclear Localization and Protein Degradation of Rac1, *Journal of Biological Chemistry*, 2004, **279**, 44197-44210.
45. D. Michaelson, W. Abidi, D. Guardavaccaro, M. Zhou, I. Ahearn, M. Pagano and M. R. Philips, Rac1 accumulates in the nucleus during the G2 phase of the cell cycle and promotes cell division, *The Journal of cell biology*, 2008, **181**, 485-496.
46. D. Michaelson, W. Abidi, D. Guardavaccaro, M. Zhou, I. Ahearn, M. Pagano and M. R. Philips, Rac1 accumulates in the nucleus during the G2 phase of the cell cycle and promotes cell division, *J Cell Biol*, 2008, **181**, 485-496.
47. S. T. Glantz, E. E. Berlew and B. Y. Chow, Synthetic cell-like membrane interfaces for probing dynamic protein-lipid interactions, *Methods in enzymology*, 2019, **622**, 249-270.
48. E. Wagner and M. Glotzer, Local RhoA activation induces cytokinetic furrows independent of spindle position and cell cycle stage, *The Journal of Cell Biology*, 2016, **213**, 641.
49. Y. Gao, J. B. Dickerson, F. Guo, J. Zheng and Y. Zheng, Rational design and characterization of a Rac GTPase-specific small molecule inhibitor, *Proceedings of the National Academy of Sciences of the United States of America*, 2004, **101**, 7618.
50. J. W. Breslin, X. E. Zhang, R. A. Worthylake and F. M. Souza-Smith, Involvement of local lamellipodia in endothelial barrier function, *PLoS One*, 2015, **10**, e0117970.
51. M. Schliwa, Action of cytochalasin D on cytoskeletal networks, *J Cell Biol*, 1982, **92**, 79-91.
52. H. Marei, A. Carpy, A. Woroniuk, C. Vennin, G. White, P. Timpson, B. Macek and A. Malliri, Differential Rac1 signalling by guanine nucleotide exchange factors implicates FLII in regulating Rac1-driven cell migration, *Nature communications*, 2016, **7**, 10664.
53. H. Marei and A. Malliri, GEFs: Dual regulation of Rac1 signaling, *Small GTPases*, 2017, **8**, 90-99.
54. L. Valon, A. Marín-Llauradó, T. Wyatt, G. Charras and X. Trepat, Optogenetic control of cellular forces and mechanotransduction, *Nature communications*, 2017, **8**, 14396.

446 **End of document**